

## Tailoring ergodicity through selective A-site doping in the $\text{Bi}_{1/2}\text{Na}_{1/2}\text{TiO}_3$ – $\text{Bi}_{1/2}\text{K}_{1/2}\text{TiO}_3$ system

Matias Acosta, Na Liu, Marco Deluca, Sabrina Heidt, Ines Ringl, Christian Dietz, Robert W. Stark, and Wook Jo

Citation: *Journal of Applied Physics* **117**, 134106 (2015); doi: 10.1063/1.4916719

View online: <http://dx.doi.org/10.1063/1.4916719>

View Table of Contents: <http://scitation.aip.org/content/aip/journal/jap/117/13?ver=pdfcov>

Published by the [AIP Publishing](#)

---

### Articles you may be interested in

[Solid-state conversion of  \$\(\text{Na}\_{1/2}\text{Bi}\_{1/2}\)\text{TiO}\_3\$ – \$\text{BaTiO}\_3\$ – \$\(\text{K}\_{1/2}\text{Na}\_{1/2}\)\text{NbO}\_3\$  single crystals and their piezoelectric properties](#)

*Appl. Phys. Lett.* **104**, 222910 (2014); 10.1063/1.4881615

[Electromechanical strain and bipolar fatigue in  \$\text{Bi}\(\text{Mg}\_{1/2}\text{Ti}\_{1/2}\)\text{O}\_3\$ – \$\(\text{Bi}\_{1/2}\text{K}\_{1/2}\)\text{TiO}\_3\$ – \$\(\text{Bi}\_{1/2}\text{Na}\_{1/2}\)\text{TiO}\_3\$  ceramics](#)

*J. Appl. Phys.* **114**, 054102 (2013); 10.1063/1.4817524

[Piezoelectricity and local structural distortions in  \$\(\text{Na}\_{0.5}\text{Bi}\_{0.5}\)\_{1-x}\text{Sr}\_x\text{TiO}\_3\$ – \$\text{Bi}\_{12}\text{TiO}\_{20}\$  flexoelectric-type polar ceramics](#)

*Appl. Phys. Lett.* **101**, 062903 (2012); 10.1063/1.4744952

[Determination of depolarization temperature of  \$\(\text{Bi}\_{1/2}\text{Na}\_{1/2}\)\text{TiO}\_3\$ -based lead-free piezoceramics](#)

*J. Appl. Phys.* **110**, 094108 (2011); 10.1063/1.3660253

[Piezoelectric and ferroelectric properties of Bi-compensated  \$\(\text{Bi}\_{1/2}\text{Na}\_{1/2}\)\text{TiO}\_3\$ – \$\(\text{Bi}\_{1/2}\text{K}\_{1/2}\)\text{TiO}\_3\$  lead-free piezoelectric ceramics](#)

*J. Appl. Phys.* **103**, 074109 (2008); 10.1063/1.2902805

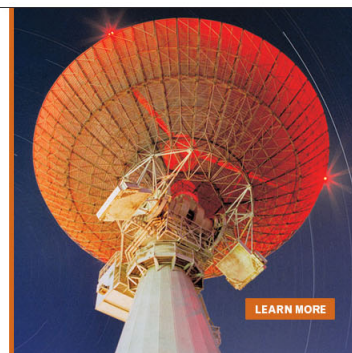
---

MIT LINCOLN  
LABORATORY  
CAREERS

Discover the satisfaction of  
innovation and service  
to the nation

- Space Control
- Air & Missile Defense
- Communications Systems & Cyber Security
- Intelligence, Surveillance and Reconnaissance Systems
- Advanced Electronics
- Tactical Systems
- Homeland Protection
- Air Traffic Control

 **LINCOLN LABORATORY**  
MASSACHUSETTS INSTITUTE OF TECHNOLOGY



## Tailoring ergodicity through selective A-site doping in the $\text{Bi}_{1/2}\text{Na}_{1/2}\text{TiO}_3\text{-Bi}_{1/2}\text{K}_{1/2}\text{TiO}_3$ system

Matias Acosta,<sup>1,a)</sup> Na Liu,<sup>2</sup> Marco Deluca,<sup>3,4</sup> Sabrina Heidt,<sup>1</sup> Ines Ringl,<sup>3,4</sup> Christian Dietz,<sup>2</sup> Robert W. Stark,<sup>2</sup> and Wook Jo<sup>1,5</sup>

<sup>1</sup>Department of Materials Science, Technische Universität Darmstadt, Alarich-Weiss-Strasse 2, 64287 Darmstadt, Germany

<sup>2</sup>Department of Materials Science and Center of Smart Interfaces, Technische Universität Darmstadt, Alarich-Weiss-Strasse 10, 64287 Darmstadt, Germany

<sup>3</sup>Materials Center Leoben Forschung GmbH, Roseggerstraße 12, Leoben A-8700, Austria

<sup>4</sup>Institut für Struktur- und Funktionskeramik, Montanuniversität Leoben, Peter Tunner Straße 5, Leoben A-8700, Austria

<sup>5</sup>School of Materials Science and Engineering, Ulsan National Institute of Science and Technology, 689-798 Ulsan, South Korea

(Received 27 October 2014; accepted 21 March 2015; published online 6 April 2015)

The morphotropic phase boundary composition  $\text{Bi}_{1/2}\text{Na}_{1/2}\text{TiO}_3\text{-}20\text{ mol. } \% \text{ Bi}_{1/2}\text{K}_{1/2}\text{TiO}_3$  was chosen as initial material to do selective A-site aliovalent doping replacing Na and K by 1 at. % La, respectively. The materials were studied macroscopically by measuring dielectric and electromechanical properties. The Na-replaced material has a lower freezing temperature  $T_{\text{fr}}$ , lower remanent polarization and remanent strain, and thus a higher degree of ergodicity than the K-replaced material. These results are contrasted with local poling experiments and hysteresis loops obtained from piezoresponse force microscopy. The faster relaxation of the tip-induced local polarization and the lower remanent state in bias-on and -off loops confirm the higher degree of ergodicity of the Na-replaced material. The difference in functional properties is attributed to small variations in chemical pressure achieved through selective doping. Raman results support this working hypothesis. © 2015 AIP Publishing LLC. [<http://dx.doi.org/10.1063/1.4916719>]

### I. INTRODUCTION

Currently, new lead-free piezoelectric ceramics for actuators applications are widely studied.<sup>1,2</sup> These efforts are driven by concerns regarding lead toxicity<sup>3,4</sup> and environmental hazards.<sup>5</sup> Therefore, there has been a continuous effort to replace  $\text{Pb}(\text{Zr},\text{Ti})\text{O}_3$  (PZT) ceramics in commercial devices such as actuators.<sup>1,2</sup> Various solid solutions in the families of bismuth-alkali-based and alkali-niobium-based systems have been investigated so far.<sup>1</sup> Among these materials, the  $\text{Bi}_{1/2}\text{Na}_{1/2}\text{TiO}_3$  (BNT)– $\text{Bi}_{1/2}\text{K}_{1/2}\text{TiO}_3$  (BKT) is a good candidate for technical applications because its properties can be engineered through proper chemical modifications.<sup>2</sup> Although La was used to modify the electrical properties of perovskite materials, its potential as dopant in BNT–BKT is not yet fully explored.

The binary solid solution BNT–BKT presents a morphotropic phase boundary (MPB) at about 18–22 mol. % BKT.<sup>6,7</sup> Several reports have focused on modifying the system through solid solutions achieving promising large signal strain properties, namely,  $d_{33}^*$  above 500 pm/V at 6 kV/mm.<sup>8–12</sup> Other studies focused on either A- and/or B-site doping to improve small and large signal electromechanical properties.<sup>13–16</sup> It was proved that either replacing Bi on the A-site<sup>16</sup> or all A-site cations are effective approaches.<sup>13</sup> Compositional modifications with iso- and aliovalent dopants are technologically relevant because small doping amounts can modify

considerably electrical properties due to cation vacancy formation and chemical pressure. Specifically, La was widely used in several archetypal perovskite materials such as  $\text{Pb}(\text{Zr},\text{Ti})\text{O}_3$ , and  $\text{Ba}_{1/2}\text{Na}_{1/2}\text{TiO}_3$ .<sup>16–18</sup> Isovalent La-doping was shown to be a viable approach to tailor the dielectric and electromechanical properties of the BNT–BKT system.<sup>13,16</sup> Nevertheless, aliovalent doping was not yet used as a strategy, neither selective doping.

Changes in degree of ergodicity, vacancies, and chemical pressure were shown to be critical in determining relaxor features.<sup>2,17–22</sup> The ergodicity term was first implemented in statistical mechanics. An ergodic property is such when the time average characteristic of it is indistinguishable from the ensemble average for the distribution of all accessible points in the phase space of the system. In other words, in an ergodic system an arbitrary function can be defined in a certain mathematical space within the phase space of the whole system, in which its characteristic becomes indistinguishable from the ensemble over all accessible points.<sup>23</sup> Expressing a higher degree of ergodicity can be understood as increasing the fraction of phase space in which its property time average characteristic becomes indistinguishable from the ensemble average for the distribution of all accessible points in the phase space of the system. Expressing a degree of non-ergodicity is therefore not a proper term but a consequence of the degree of ergodicity. However, we use this term throughout the manuscript to distinguish considerable changes in the degree of ergodicity. Considering that there has been reports demonstrating only a certain degree of

<sup>a)</sup>Email: [acosta@ceramics.tu-darmstadt.de](mailto:acosta@ceramics.tu-darmstadt.de). Telephone: +49 (0)6151 16-6312.

ergodicity,<sup>24</sup> understanding the properties and structure locally and macroscopically is key for assessing a complete physical view.

Piezoresponse force microscopy (PFM) and Raman scattering have proven to be powerful experimental techniques to elucidate microscopic piezoelectric properties and resolve the local structure in lead-free piezoceramics.<sup>25–29</sup> PFM has been widely applied to study ferroelectric domains on the nanoscale.<sup>27,30</sup> As other scanning probe microscopy techniques, PFM allows for a lateral resolution of a few tens of nanometers and is characterized by its sensitivity to the local polarization when an external electrical field is applied to a conductive tip. This facilitates the potential to investigate local phenomena behind the functionality of relaxors on the nanoscale such as the existence of polar nanoregions (PNRs).<sup>31</sup> Additionally, local hysteresis loops and local poling experiments can be performed on particular positions of the sample<sup>26</sup> allowing to obtain information about the local remnant polarization and relaxation behavior.<sup>25</sup> In contrast, Raman spectroscopy is very useful to study the structural changes occurring on a short range owing to its coherence length down to the nanometer scale. Therefore, it offers the ability to combine the results with the nanoscale functional properties obtained by PFM.<sup>28</sup> The gathered information with these techniques is of particular importance for BNT-based materials, which are characterized by a high degree of structural disorder.<sup>32</sup> Raman spectroscopy can visualize phase transitions or short-range structural rearrangements as a function of composition,<sup>33–35</sup> temperature,<sup>36</sup> or applied electric-field.<sup>29</sup> Nevertheless, a distinction between chemically ordered regions and PNRs is not feasible solely by Raman spectroscopy. Hence, both techniques allow for observation of complementary information about local microstructural features.

In this study, the A-site doping replacing Na and K by 1 at. % La on the BNT–20BKT system is reported. The effects of the selective aliovalent doping are investigated by means of macroscopic dielectric and electromechanical properties. The dielectric properties indicate that the Na-replaced material presents a lower freezing temperature and thus a higher degree of ergodicity at room temperature. This result is corroborated by a lower macroscopic remanent polarization and local features such as faster tip-induced poling relaxation and lower remanent state in bias-off experiments. It is suggested that the different dielectric and electromechanical properties of both materials are due to small differences in chemical pressure in the Na-replaced as suggested by Raman spectroscopy and in qualitative agreement with hydrostatic measurements in archetypal relaxors. Therefore, a correlation between local techniques such as PFM and Raman spectroscopy and macroscopic functional properties is obtained. It is shown that selective aliovalent doping can be used to modify relaxor features locally, thus giving the possibility of engineering macroscopic lead-free relaxor piezoceramics.

## II. EXPERIMENTAL

The MPB of the  $0.8\text{Bi}_{1/2}\text{N}_{1/2}\text{TiO}_3\text{--}0.2\text{Bi}_{1/2}\text{K}_{1/2}\text{TiO}_3$  (BNKT) system<sup>6,7</sup> was chosen as initial material. Two variants were designed replacing Na and K by 1 and 3 at. % La, leading

to the stoichiometric formulas  $\text{Bi}_{0.5}\text{Na}_{0.39}\text{K}_{0.1}\text{La}_{0.01}\text{TiO}_3$  (BN0.39KLT) and  $\text{Bi}_{0.5}\text{Na}_{0.4}\text{K}_{0.09}\text{La}_{0.01}\text{TiO}_3$  (BNK0.09LT), respectively. The materials were prepared by a conventional solid state route using  $\text{Bi}_2\text{O}_3$  (99.975%),  $\text{Na}_2\text{CO}_3$  (99.5%),  $\text{K}_2\text{CO}_3$  (99.0%), and  $\text{La}_2\text{O}_3$  (99.9%) as raw materials (Alfa Aesar GmbH & Co., Germany). Calcination was done at 850 °C for 3 h and sintering at 1150 °C for 2 h. Further details on the processing route can be found elsewhere.<sup>37</sup> In order to highlight the importance of selective acceptor doping, functional properties in the 1 at. %-doped compositions will be presented. Nevertheless, the reader should be aware that results of the selective doping remain valid for 3 at. %-doped compositions.

The densities were measured by the classical Archimedes method. For the microstructure investigation, sintered samples were polished in a semi-automatic machine (Jean Wirtz, Phoenix 4000, Germany). Afterwards, the samples were thermally etched at 940 °C for 30 min with a heating rate of 10 °C/min. To ensure conductive surfaces, all samples were sputtered with silver (Gwent Electronic Materials, Ltd., C60704D8, United Kingdom). Imaging was performed in a scanning electron microscope (SEM) (Philips, XL 30 FEG, Netherlands). The average grain size was obtained by the mean intercept length method with a numerical multiplication factor of 1.56.<sup>38</sup>

A commercial impedance analyzer (Novocontrol Technologies, Impedance analyzer Alpha-A, Germany) equipped with a cryostat was used for the temperature- and frequency-dependent real relative permittivity  $\epsilon_r'$  of the unpoled samples during cooling. Frequencies ranging from  $10^{-1}$  to  $10^6$  Hz with amplitude of 1 V in the temperature range from –150 to 250 °C and a cooling rate of 1 K/min were employed.

For the polarization and strain measurements, virgin samples were used. A function generator (Agilent Corporation, 33220A, U.S.) supplied an input bipolar signal to a voltage amplifier (Trek, High Voltage Amplifier 20/20 C, U.S.) for the macroscopic electrical characterization of the specimens. This resulted in an electric-field strength of 6 kV/mm and 1 Hz. The polarization at room temperature was measured with a standard Sawyer-Tower circuit with a measuring capacitor of 10  $\mu\text{F}$ . At the same setup, strain was measured by an optical sensor (Philtec, D63, U.S.).

A Cypher atomic force microscope with Ti/Ir (5/20) coated conductive cantilevers ASYELEC-01 (both from Asylum Research, U.S.) was used for the PFM study. The nominal spring constant of this type of cantilevers was  $k = 2$  N/m with a nominal fundamental resonance frequency  $f_0 = 70$  kHz. All PFM images were acquired on mirror-polished sample surfaces (polishing down to  $1/4$   $\mu\text{m}$ ) using the dual alternating current resonance tracking (DART) mode provided by the microscope manufacturer. Using the contact resonance imaging technique, the recorded amplitudes indicated the magnitude of the local effective piezoelectric constant  $d_{33}$  beneath the tip whereas the phase shift between the mechanical oscillation and the electrical stimulus was used to determine the orientation of the polarization of the sample with respect to the applied electric-field. PFM images with a resolution of  $(256 \times 256)$  pixel using a constant loading force of approximately  $F = 120$  nN were

acquired. A peak-to-peak driving voltage of 6 V was applied to the tip while scanning perpendicular to the length axis of the cantilever with a velocity of 5  $\mu\text{m/s}$ . Local areas of  $(1 \times 1) \mu\text{m}^2$  were poled by scanning the sample surface line-wise with a tip velocity of 5  $\mu\text{m/s}$  and simultaneously applying a direct voltage of  $-10$  V.

Local hysteresis loops on the sample surface were acquired by the switching spectroscopy PFM method in DART mode.<sup>39</sup> An alternating current voltage (2 V peak-to-peak) was superimposed to a bias voltage. The bias served for the local poling of the sample at specific locations. The alternating current was used for the simultaneous read-out of the piezoresponse. In the DART mode, this alternating current signal is a combination of two frequencies, one below and one above the contact resonance frequency that is constantly tracked by an additional feedback loop. The bias describes a sinusoidal-like function (16 V peak-to-peak) starting from initially 0 V with a stepwise increasing/decreasing rectangular pulse including an off-state after each poling step. The oscillation amplitude/phase during the bias-on and bias-off states was read out to measure the piezoelectric response of the surface. A pulse time of 25 ms in 100 steps was chosen for each oscillation cycle with a bias-off time equal to the pulse time. The scan direction was from top to bottom, and the acquisition time for one image was approximately 8 min. The bias-on and bias-off hysteresis loops both can be read out by SS-PFM. The bias-off hysteresis loops are related to the remanent piezoresponse signal measured between the consecutive dc bias steps with the dc bias switched off. The bias-on hysteresis loops, however, are influenced by the electrostatic interactions generated by the electrical field beneath the tip.<sup>39</sup> This leads to a substantially lower coercive voltage,<sup>40</sup> a higher slope and response compared to the off-state including an inversion of the loops.<sup>40</sup> The on- and off-state loops were obtained at the same sample positions. As a result, the electrostatic influence of the applied electrical field on the piezoresponse signal can be extracted. Furthermore, the hysteresis loops obtained on the different samples were recorded under same experimental conditions; hence, they are relatively comparable to each other.

Topography images were first-order flattened, all other images were leveled by a line-wise offset subtraction. For the hysteresis loops, a total number of seven cycles per position were averaged to achieve the final hysteresis loops representative for each sample. An estimate for the effective piezoelectric coefficient  $d_{33}$  was calculated, as given in the below equation

$$d_{33} = A \cos(\phi) / V_{ac}, \quad (1)$$

where  $A$  is the amplitude of the cantilever oscillation,  $\phi$  is the respective phase shift between the mechanical oscillation and the electrical excitation of the cantilever when the tip interacts with the sample surface, and  $V_{ac}$  is the applied alternating voltage to the tip.

Raman measurements were performed on a LabRAM spectrometer (Horiba Jobin Yvon, France) with 532 nm (frequency doubled Nd:YAG) laser excitation. Laser power was kept below 5 mW to avoid substantial heating on the sample.

The laser was focused on the surface of the samples by means of a long-working distance objective with  $100\times$  magnification and a numerical aperture of 0.8. Spectral resolution was  $1.5 \text{ cm}^{-1}/\text{pixel}$  (numerical grating 1800 g/mm). The acquired spectra were averaged on a minimum of 5 repetitions in order to improve the signal-to-noise ratio. Each spectrum was measured three times with an integration time of 0.5 s. Consequently, spectra were smoothed and normalized using a commercial software (Labspec 6, Horiba Jobin Yvon, France).

### III. RESULTS AND DISCUSSION

#### A. Effect of chemical substitution on microstructure

Density and grain size analysis did not show differences between BN0.39KLT and BNK0.09LT. Both materials presented relative densities above 97% and grain sizes of approximately 1.3  $\mu\text{m}$ . Similar densities were reported in other La-doped materials and were related to the presence of La-cation complex defects aiding the sintering process.<sup>41,42</sup>

The X-ray diffraction patterns of both materials showed a single pseudocubic perovskite structure. This is consistent with the results found in the literature in similar lead-free materials with little non-cubic distortions.<sup>43</sup> This measurement reveals the representative macroscopic average structure. Nevertheless, the detection of a Raman spectrum in such materials is a proof that the structure at the unit cell scale is not centrosymmetric,<sup>33</sup> as will be presented in Section III D. Average structure of BNKT also resembles that of La-modified BNKT. Non-cubic distortions are hardly distinguishable because they are very low<sup>43</sup> and thus below the resolution limit of our setup. A detailed structural investigation of these materials is out of the scope of the present paper, but it will be considered for future investigations.

Since La diffused into the lattice, either formation of cation vacancies, reduced concentration of oxygen vacancies or free electrons should develop during the incorporation process<sup>42</sup> to compensate the charge of the aliovalent doping. Previous reports in La-doped perovskites showed that  $\text{La}^{3+}$  is exclusively incorporated on the A-site.<sup>42,44,45</sup> In the case of BNT–BKT, there are different A-site cation replacement possibilities. *A priori*, it can be thought that  $\text{La}^{3+}$  would replace  $\text{Bi}^{3+}$  cations on the A-site taking into account oxidation state, similar radii ( $\text{Bi}^{3+} \sim 1.32$ ,  $\text{Na}^+ \sim 1.39$ ,  $\text{K}^+ \sim 1.64$ , and  $\text{La}^{3+} \sim 1.36 \text{ \AA}$  (Ref. 46)), and the non-negligible volatilization of  $\text{Bi}^{3+}$  during calcination and sintering.<sup>47</sup> Nevertheless, the macroscopic properties of BNT–BKT system with  $\text{La}^{3+}$  entering into Bi-sites differ considerably from the materials presented here.<sup>15</sup> Therefore, we presume that  $\text{La}^{3+}$  entered into the lattice in the chosen deficient sites of  $\text{Na}^+$  and  $\text{K}^+$  for the BN0.39KLT and BNK0.09LT, respectively. The most feasible charge compensation is thus by the creation of  $\text{K}^+$  and  $\text{Na}^+$  cation vacancies,<sup>18,42</sup> as given in the below equation



The presented reaction is expected taking into account that alkali cations tend to volatilize during sintering, and their non-stoichiometry is encountered in many lead-free systems.<sup>41,47,48</sup> Although we already discarded the possibility of

exclusive  $\text{Bi}^{3+}$  replacement by  $\text{La}^{3+}$ , we cannot neglect the compensation of pairs of  $(\text{Bi}^{3+}, \text{Na}^+)$  and  $(\text{Bi}^{3+}, \text{K}^+)$  for BN0.39KLT and BNK0.09LT, nor electronic compensation, nor a decrease in oxygen vacancy concentration. As it will be seen in Section III B, there have not been clear differences in the conductivity of BN0.39KLT and BNK0.09LT, and thus, cation compensation seems to be responsible for charge compensation. However, there is no driving force for different charge compensation mechanisms in BN0.39KLT and BNK0.09LT. Further inquiries on defect stoichiometry are out of the scope of the present paper and left for future work. Nevertheless, clear differences in macroscopic physical features of both materials are observed leading to the conclusion that changes in electromechanical are related to the presence of La in the system entering into different lattice sites.

## B. Dielectric and electromechanical properties

Fig. 1 introduces the  $\epsilon_r'$  values as function of temperature and frequency. A frequency dependent anomaly at approximately 345 K and 355 K is observed for BN0.39KLT (a) and BNK0.09LT (b), respectively. This anomaly shifts to higher temperatures and decreases its magnitude with increasing frequency, which indicates relaxor properties in both materials.<sup>49</sup> This behavior is also common to other lead-free materials<sup>37,50,51</sup> and was associated with the relaxation of PNRs fluctuations, i.e., a dynamic slowing down of PNRs thermally activated fluctuations.<sup>50</sup> Therefore, with further temperature decrease either a spontaneous transformation into a long-range ferroelectric order (non-canon relaxor) or freezing of the PNRs fluctuations (canonic relaxor) can be expected.<sup>52</sup> There is no indication of a transformation into a long-range order ferroelectric state, and thus, we classify these materials as canonic relaxors. It was proposed that the freezing of PNRs can be rationalized by the Vogel–Fulcher<sup>53,54</sup> relationship.<sup>55</sup> Fig. 2 presents the freezing temperatures ( $T_{\text{fr}}$ ) of both materials calculated from the local maxima  $\epsilon_r'$  values fitted with the Vogel–Fulcher<sup>53,54</sup> relationship. The  $T_{\text{fr}}$  for BN0.39KLT is  $(253 \pm 12)$  K, while for BNK0.09LT, it is  $(283 \pm 9)$  K. Because in both cases  $T_{\text{fr}}$  is close to room temperature, ergodic and non-ergodic states may coexist in these material. We stress here that we refer to a difference in the local degree of ergodicity and not necessarily to two different macroscopic phases with different relaxor states. Different degree of ergodicity was already found in similar lead-free materials both macroscopically<sup>24,51</sup> and microscopically.<sup>56</sup> Given the difference in freezing temperatures, BN0.39KLT should present a higher degree

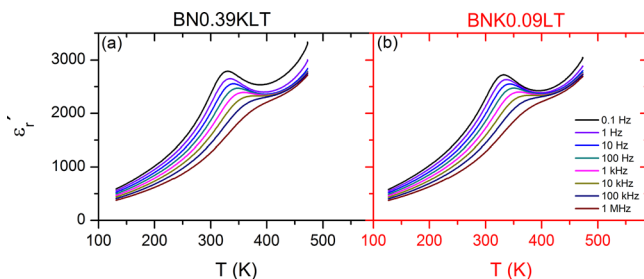


FIG. 1. Real part of the relative permittivity of (a) BN0.39KLT (black) and (b) BNK0.09LT (red).

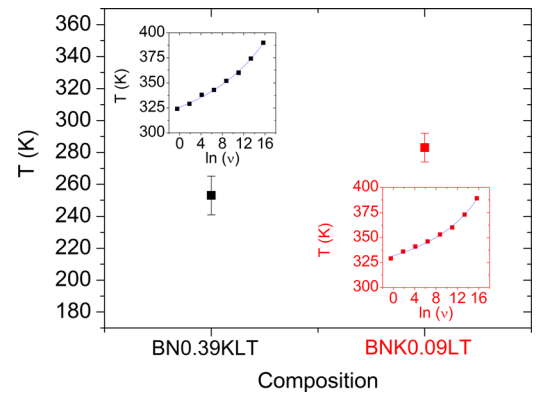


FIG. 2. Freezing temperature obtained from Vogel–Fulcher fitting for BN0.39KLT (black) and BNK0.09LT (red). Insets display the fitting curves utilized to determine  $T_{\text{fr}}$ .

of ergodicity at room temperature in comparison to BNK0.09LT. Pure BNKT at its MPB presents a  $T_{\text{fr}}$  corresponding to  $(315 \pm 5)$  K (not shown). Therefore, the pure MPB material is expected to present the lowest degree of ergodicity at room temperature.

Macroscopically bipolar polarization and strain loops obtained on virgin specimens are presented in Fig. 3 together with pure BNKT for comparison. Pure BNKT presents a remanent polarization  $P_r = 0.26$  C/m<sup>2</sup> and maximum polarization at 6 kV/mm is  $P_{\text{max}} = 0.36$  C/m<sup>2</sup>. For BN0.39KLT, the remanent polarization is  $P_r = 0.17$  C/m<sup>2</sup> and the maximum polarization at 6 kV/mm is,  $P_{\text{max}} = 0.35$  C/m<sup>2</sup>. For BNK0.09LT, a  $P_r = 0.24$  C/m<sup>2</sup> and  $P_{\text{max}} = 0.36$  C/m<sup>2</sup> were measured. The  $P_r$  of BN0.39KLT is  $\sim 35\%$  lower than in BNKT and  $\sim 30\%$  lower than in BNK0.09LT. In all materials  $P_{\text{max}}$  values are within 5% difference. The lowest  $P_r$  in the BN0.39KLT material results from the more pronounced pinching of the polarization loop.

The strain curves indicate that BNKT presents a remanent strain of  $S_r = 0.26\%$ , an irreversible strain of  $S_{\text{irr}} = 0.13\%$ , and a maximum strain of  $S_{\text{max}} = 0.44\%$  at 6 kV/mm. The BN0.39KLT presents a remanent strain of  $S_r = 0.13\%$ , an irreversible strain of  $S_{\text{irr}} = 0.02\%$ , and a maximum strain of  $S_{\text{max}} = 0.4\%$  at 6 kV/mm. The BNK0.09LT presents  $S_r = 0.22\%$ ,  $S_{\text{irr}} = 0.1\%$ , and  $S_{\text{max}} = 0.41\%$ .  $S_{\text{max}}$  is similar in both materials doped materials and slightly larger in BNKT, which is consistent with polarization measurements. However, the BN0.39KLT presents a decrease of 40% in  $S_r$  and 20% in  $S_{\text{irr}}$  in comparison to BNK0.09LT. Moreover, if compared to pure BNKT, BNK0.09LT presents  $\sim 15\%$  in  $S_r$  and  $S_{\text{irr}}$ . Reduced  $P_r$ ,  $S_r$ , and  $S_{\text{irr}}$  are common features observed in lead-free materials with increased ergodicity.<sup>2</sup> Therefore, the BN0.39KLT presents the highest

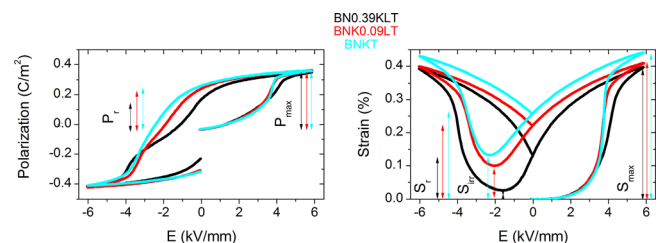


FIG. 3. (a) Polarization and (b) strain curves on a virgin state for BN0.39KLT (black) and BNK0.09LT (red).

degree of ergodicity, followed by BNK0.09LT and BNKT. This observation is in agreement with the calculated  $T_{fr}$  of all the materials. Interestingly, for large signal electromechanical applications, BN0.39KLT presents one of the highest strain responses reported so far resulting in an exemplary candidate for actuator applications.<sup>2</sup>

Since we expect similar defect chemistry in both materials (Eq. (2)), the difference in ergodicity may result from local chemical pressure changes<sup>20</sup> exerted by the difference in the A-site cation radii upon doping. In BaTiO<sub>3</sub>, it was experimentally shown that a similar qualitative shift of  $T_c$  was obtained by modifying the system with Sr-doping or applying an hydrostatic pressure, indicating similarities between chemical and hydrostatic pressure.<sup>57</sup> Theoretical calculations showed that hydrostatic pressure mostly modifies bond lengths and slightly affects tilting angles, suggesting that these microstructural rearrangements are responsible of the functional properties modification.<sup>21,22</sup> However, in archetypal relaxors, it was also shown experimentally that tilting angles change at sufficient high pressures<sup>58</sup> and lead to oxygen anisotropic displacements.<sup>59</sup> These structural changes were also reflected in the change of dielectric and electromechanical properties under hydrostatic pressure in relaxors, as reported in several works by Samara *et al.*<sup>60–65</sup> Specifically, it was shown that with the increase in hydrostatic pressure, the thermal relaxation of PNRs occurred gradually at lower temperatures.<sup>60,66,67</sup> This behavior indicates a qualitative correlation with the chemical pressure exerted in this work due to selective La-doping and hydrostatic pressure in archetypal relaxors. We hypothesize that the BNT–BKT reduces its chemical pressure locally when K<sup>+</sup> is replaced due to its larger ionic radius in comparison to the similar radii of Bi<sup>3+</sup>, Na<sup>+</sup>, and La<sup>3+</sup>. In other words, BN0.49KLT presents a higher local chemical pressure, and thus, its dielectric thermal relaxation, rationalized with  $T_{fr}$ , is expected at lower temperatures (Fig. 2). The changes in the local chemical pressure should be small because the maximum values of the dielectric properties (Fig. 1) remain similar, which is in agreement with low hydrostatic pressures.<sup>60</sup> This result indicates that the functional properties of the MPB of BNT–BKT should be quite sensitive to hydrostatic pressures. In order to probe locally the physical features of doped materials, PFM and Raman spectroscopy are presented subsequently. It should be pointed out that the concepts related to degree of ergodicity in Sections III C and III D could be extrapolated to the pure BNKT based on the presented macroscopic results. However, to the authors' knowledge, a detailed microscopic study of the MPB of the BNKT system is missing in literature and remains as future work.

### C. Piezoresponse force microscopy

Fig. 4 shows piezoresponse images ( $5 \times 5$ )  $\mu\text{m}^2$  of the virgin domain state of BN0.39KLT (a)–(c) and BNK0.09LT (d)–(f), respectively. The averaged root mean squared roughness (calculated from three images of each sample) was approximately  $(1.5 \pm 0.5)$  nm and  $(1.6 \pm 0.3)$  nm for the BN0.39KLT and BNK0.09LT, respectively. The relatively low surface roughness for both samples suggests a minor

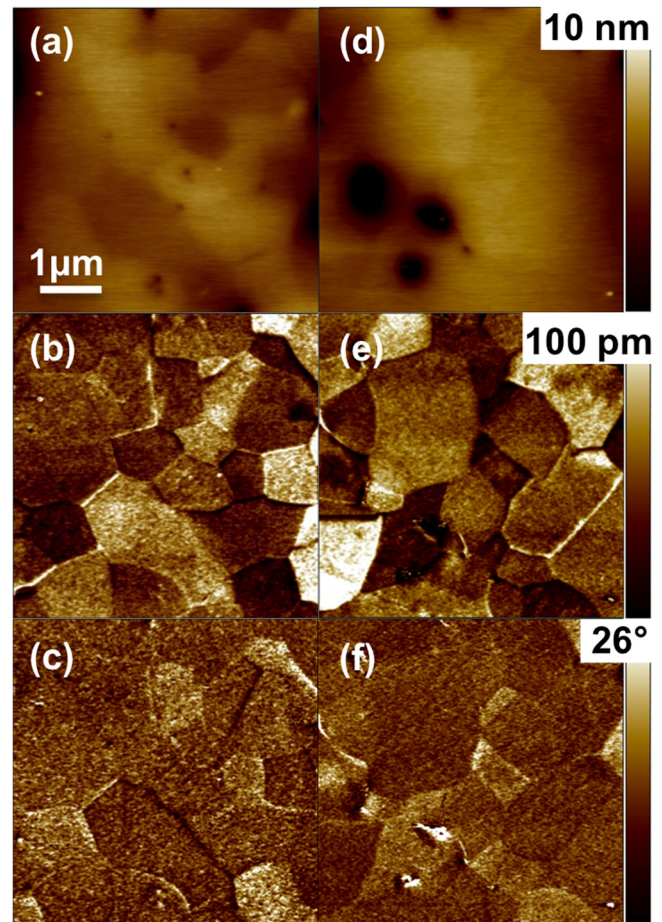


FIG. 4. (a) and (d) Topography, amplitude images ((b) and (e)) and phase response ((c) and (f)) of the initial domain state of a BN0.39KLT ((a)–(c)) and BNK0.09LT sample ((d)–(f)) measured by PFM in the DART mode.

crosstalk between topography and amplitude/phase channels. Figs. 4(b) and 4(e) correspond to the amplitude and Figs. 4(c) and 4(f) to the phase responses of the BN0.39KLT and BNK0.09LT, respectively. The amplitude response images of the initial state (Figs. 4(b) and 4(e)) depict regions with distinctive amplitude values on the size of a few micrometers for both samples. The phase response images of the initial state (Figs. 4(c) and 4(f)), however, do not show the clear contrast. The absence of the contrast and the associated phase alignment is typical for relaxors and was previously shown in similar lead-free systems.<sup>25</sup> The typical PNRs of these relaxor materials can hardly be resolved by the conductive AFM tip.<sup>68</sup>

To pole a certain area ( $1 \times 1$ )  $\mu\text{m}^2$ , we applied an input dc voltage of  $-10$  V while line-wise scanning the sample surface in the contact mode. The associated electric-field was sufficient to partially induce ferroelectric domains with an orientation perpendicular to the sample surface. Figs. 5(a)–5(d) (BN0.39KLT) and Figs. 5(e)–5(h) (BNK0.09LT) show an image series of the local relaxation process with the amplitude ((a) and (e)) and phase response ((b) and (f)) captured immediately after the poling and the respective amplitude/phase response (“(c) and (g)” and “(d) and (h)”) captured 60 min after poling. Immediately after the poling, approximately 80% of the poled area in the phase response

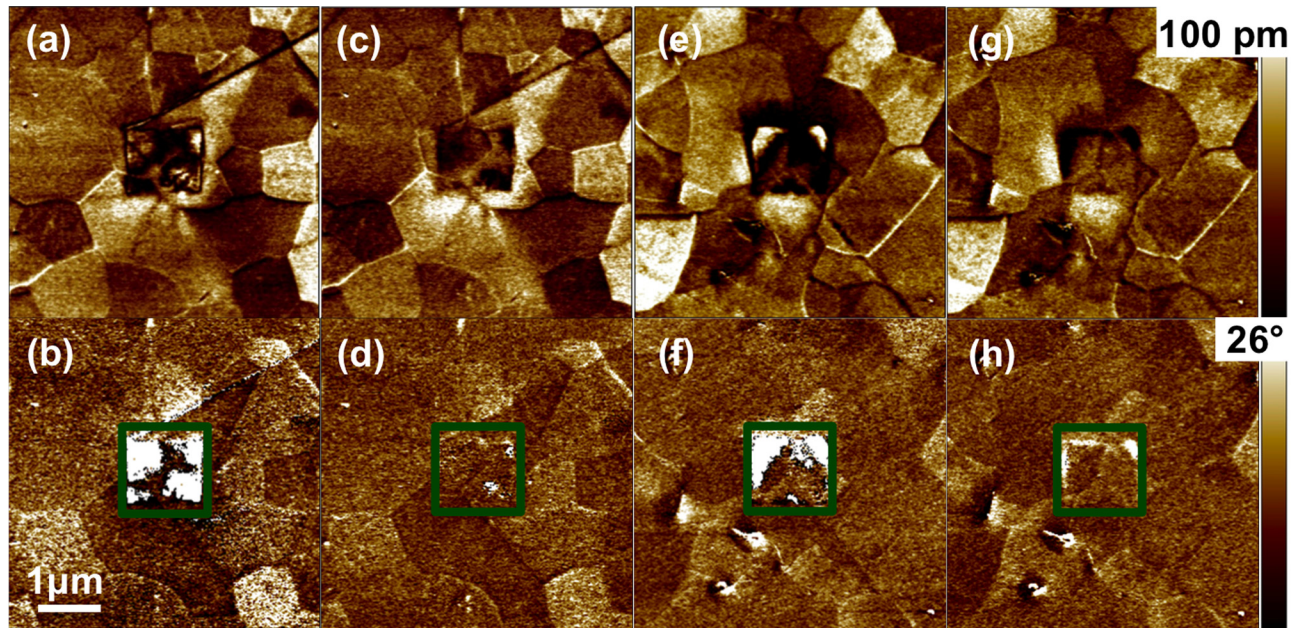


FIG. 5. Relaxation process of BN0.39KLT ((a)–(d)) and BNK0.09LT ((e)–(h)) after a local poling experiment measured by PFM in the DART mode. (a) and (e) Amplitude and (b)–(f) phase response subsequently imaged after poling a  $(1 \times 1) \mu\text{m}^2$  region in the center (enclosed by the green frame); (c) and (g) amplitude and (d) and (h) phase response imaged 60 min after poling, respectively. For a better visibility of the piezoresponse, the color bar of the phase images was set to a range smaller than the total recorded phase shift. The values of the white area within the green frames of the phase images (b), (d), (f), and (h) correspond to approximately  $180^\circ$ .

of the BN0.39KLT sample (Fig. 5(b)) changed to  $180^\circ$ . In contrast, only 50% of the framed area (Fig. 5(f)) of the BNK0.09LT sample could be poled. The majority of the poled areas of both samples relaxed back to the initial domain state as detected 60 min after subsequent PFM imaging (“Figs. 5(c) and 5(d)” and “Figs. 5(g) and 5(h)”). Compared to the BN0.39KLT sample, a larger region at the upper side of the poling area of the remaining tip-induced domain was observed for the BNK0.09LT sample. The results demonstrate that ferroelectric domains could be induced in both samples. However, the tip-induced ferroelectric domains of both samples were unstable with time. A faster relaxation was observed for the BN0.39KLT sample and a larger long-range ordered domain could be initially induced compared to the BNK0.09LT sample. These results are attributed to the higher ergodicity of BN0.39KLT. It was already shown that

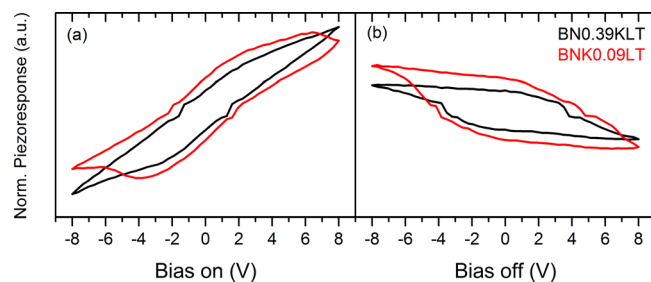


FIG. 6. Local hysteresis loops acquired on single spots applying the switching spectroscopy PFM mode with (a) bias-on and (b) bias-off for BN0.39KLT (black) and BNK0.09LT (red). Each loop is an average of 7 single loops taken at the same spot on the sample surface. The normalized piezoresponse (Norm. Piezoresponse, proportional to the effective piezoelectric coefficient  $d_{33}$ ) was calculated from the product of the amplitude and the sine of the phase shift divided by the ac driving voltage. It was normalized by the maximum piezoresponse obtained on BN0.39KLT (bias-on). Scales in (a) and (b) are comparable to each other.

materials with a high degree of ergodicity present incipient features and high-electromechanical response.<sup>2,51,69</sup>

Fig. 6 shows the averaged local hysteresis loops obtained on BN0.39KLT and BNK0.09LT samples with bias switched on (a) and off (b). The bias-on hysteresis loops reveal that the maximum local strain value of the BN0.39KLT is higher than that of the BNK0.09LT, consistent with macroscopic measurements (Fig. 3). The bias-off, i.e., the remnant piezoresponse signal, results gave the opposite tendency. In both graphs, we found a larger remnant polarization for the BNK0.09LT sample. This phenomenon is also consistent with the macroscopic large signal measurements, indicating that because of the lower ergodicity of BNK0.09LT, the remnant polarization and strain are macroscopically and microscopically retained in this material.

The reason for the discrepancy between bias-off and bias-on hysteresis loops can be explained by the increased tendency to back-switch domains in case of the BN0.39KLT compared with the BNK0.09LT, as observed in the poling experiment in Fig. 3. This finding, together with the larger remnant polarization, corroborates the higher ergodicity of the BN0.39KLT. By analyzing  $T_{fr}$  of both materials, it was also revealed a higher ergodicity in BN0.39KLT as well. These results are in good agreement with the nanoscopic observations. The relaxation behavior of both samples demonstrates that a high electric-field can induce macroscopic ferroelectric domains in both relaxor surfaces.

#### D. Raman scattering

Room-temperature Raman spectra of BN0.39KLT and BNK0.09LT are shown in Fig. 7. The spectral signature was consistent with that of BNT-based materials, and was

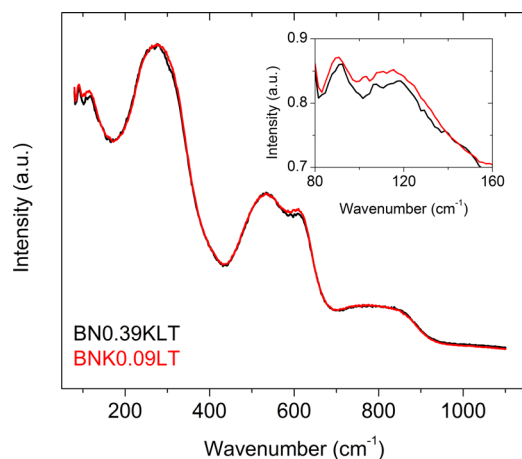


FIG. 7. Room-temperature Raman spectra of BN0.39KLT (black) and BNK0.09LT (red). In the inset the mode at  $\sim 135\text{ cm}^{-1}$  related to A-site Na/K-O vibrations is shown. The mode at  $\sim 270\text{ cm}^{-1}$  is ascribed to Ti–O vibrations, whereas above  $400\text{ cm}^{-1}$ ,  $\text{BO}_6$  polyhedral vibrational modes are located. The overall broad spectral signature is an indication of intrinsic translational disorder.

dominated by translational disorder, visible by the overall broad spectral appearance.<sup>28,29,70</sup> The peak at  $\sim 135\text{ cm}^{-1}$  (shown in the inset of Fig. 7) is ascribed to a two-mode behavior of Na- and K-based chemical clusters,<sup>28</sup> and thus is influenced by A-site doping. Experimental confirmation of chemical clusters in ferroelectrics was performed very recently,<sup>71</sup> in agreement with the described two-mode behavior. Also, the Ti–O mode at  $\sim 270\text{ cm}^{-1}$  and the higher wavenumber (oxygen-related) modes can be influenced by chemical substitution, because replacement of a cation with different size at the A-site produces distortion of the unit cell.<sup>28</sup> Nevertheless, no clear differences could be observed between the spectra of both specimens. We interpreted this as due to the small substituent amount. The width of Raman modes is a distinctive trait of the short-range order/disorder state of a material.<sup>72</sup> Higher doping contents are needed to produce changes that can be distinguished from the overall broad spectrum on which they are superposed due to intrinsic disorder.<sup>33</sup> Only slight changes in the spectra of BN0.39KLT and BNK0.09LT were observed. A slight shifting of the mode at  $135\text{ cm}^{-1}$  and the mode at  $270\text{ cm}^{-1}$  was observed. This may be attributed to a small degree of chemical pressure, which would be consistent with the low chemical pressure depicted from dielectric measurements (Fig. 1). Nevertheless, it must be highlighted that changes in Raman spectra are rather small. Further investigations are being conducted to quantify the chemical pressure and their influence in the physical features of the system. However, it should be emphasized that the exerted chemical pressure was high enough to modify considerably the microscopic and macroscopic functional properties of the BNKT system.

#### IV. CONCLUSIONS

The functional properties of BNT–BKT change drastically through selective A-site doping. Replacing Na by 1 at. % La resulted in an attractive material for actuator

applications with a high recoverable strain that is attributed to its high degree of ergodicity. In contrast, replacing K by 1 at. % La resulted in a material with a higher freezing temperature and thus higher degree of non-ergodicity and remanent state. The macroscopic properties are corroborated by local measurements obtained from piezoresponse force microscopy. The higher degree of ergodicity of the Na-replaced material is reflected in a higher degree of locally induced switching, as well as a faster relaxation at room temperature. Furthermore, measuring the local hysteresis loops revealed a higher piezoresponse in the Na-replaced material under bias-on and a lower remanent state under bias-off. The different functional properties are attributed to small variations of the chemical pressure. We hypothesize that the chemical pressure of the K-replaced material is reduced due to the lower amount of  $\text{K}^+$  that presents the highest cation radius.

Our results indicate that not only the concentration and cation used for iso- or aliovalent doping has to be considered but also the crystallographic site chosen for the dopant may be critical in future investigations. This approach gives an extra degree of freedom for engineering functional properties of complex A- and B-site lead-free piezoceramics.

#### ACKNOWLEDGMENTS

This work was supported by the Deutsche Forschungsgemeinschaft through the Sonderforschungsbereich 595/D6 “Electrical Fatigue in Functional Materials” and the AdRIA Hesse state center for Adaptronics.

- <sup>1</sup>J. Rödel, W. Jo, K. T. P. Seifert, E.-M. Anton, T. Granzow, and D. Damjanovic, *J. Am. Ceram. Soc.* **92**, 1153 (2009).
- <sup>2</sup>W. Jo, R. Dittmer, M. Acosta, J. Zang, C. Groh, E. Sapper, K. Wang, and J. Rödel, *J. Electroceram.* **29**, 71 (2012).
- <sup>3</sup>P. N. D. Lyn, *Altern. Med. Rev.* **11**, 2 (2006).
- <sup>4</sup>W. J. Foster, J. K. Meen, and D. A. Fox, *Cutaneous Ocul. Toxicol.* **32**, 18 (2013).
- <sup>5</sup>Off. J. Eur. Union: Legis. **174**, 88 (2011).
- <sup>6</sup>A. Sasaki, T. Chiba, T. Mamiya, and E. Otsuki, *Jpn. J. Appl. Phys.* **38**, 5564 (1999).
- <sup>7</sup>Y. Hiruma, K. Yoshii, H. Nagata, and T. Takenaka, *J. Appl. Phys.* **103**, 084121 (2008).
- <sup>8</sup>N.-B. Do, H.-B. Lee, C.-H. Yoon, J.-K. Kang, J.-S. Lee, and I.-W. Kim, *Trans. Electr. Electron. Mater.* **12**, 64 (2011).
- <sup>9</sup>A. Hussain, C. W. Ahn, A. Ullah, J. S. Lee, and I. W. Kim, *Jpn. J. Appl. Phys.* **49**, 041504 (2010).
- <sup>10</sup>A. Hussain, C. W. Ahn, J. S. Lee, A. Ullah, and I. W. Kim, *Sens. Actuators, A* **158**, 84 (2010).
- <sup>11</sup>A. Ullah, C. W. Ahn, A. Hussain, S. Y. Lee, and I. W. Kim, *J. Am. Ceram. Soc.* **94**, 3915 (2011).
- <sup>12</sup>A. Ullah, C. W. Ahn, A. Hussain, S. Y. Lee, H. J. Lee, and I. W. Kim, *Curr. Appl. Phys.* **10**, 1174 (2010).
- <sup>13</sup>T. H. Dinh, H.-Y. Lee, C.-H. Yoon, R. A. Malik, Y.-M. Kong, and J.-S. Lee, *J. Korean Phys. Soc.* **62**, 1004 (2013).
- <sup>14</sup>J. Yoo, J. Hong, H. Lee, Y. Jeong, B. Lee, H. Song, and J. Kwon, *Sens. Actuators, A* **126**, 41 (2006).
- <sup>15</sup>B. Wang, L. Luo, F. Ni, P. Du, W. Li, and H. Chen, *J. Alloys Compd.* **526**, 79 (2012).
- <sup>16</sup>Q. Zheng, C. Xu, D. Lin, D. Gao, and K. W. Kwok, *J. Phys. D: Appl. Phys.* **41**, 125411 (2008).
- <sup>17</sup>X. Dai, Z. Xu, and D. Viehland, *Philos. Mag. B* **70**, 33 (1994).
- <sup>18</sup>J.-K. Lee, J. Y. Yi, and K. S. Hong, *J. Appl. Phys.* **96**, 1174 (2004).
- <sup>19</sup>F. Chu, N. Setter, and A. K. Tagantsev, *J. Appl. Phys.* **74**, 5129 (1993).
- <sup>20</sup>D. C. Fredrickson, *J. Am. Chem. Soc.* **134**, 5991 (2012).
- <sup>21</sup>H. J. Zhao, W. Ren, Y. Yang, X. M. Chen, and L. Bellaiche, *J. Phys.: Condens. Matter* **25**, 466002 (2013).

- <sup>22</sup>H. J. Zhao, W. Ren, X. M. Chen, and L. Bellaiche, *J. Phys.: Condens. Matter* **25**, 385604 (2013).
- <sup>23</sup>T. Komatsuzaki, A. Baba, S. Kawai, M. Toda, J. E. Straub, and R. S. Berry, *Advancing Theory for Kinetics and Dynamics of Complex, Many-Dimensional Systems: Clusters and Proteins* (John Wiley & Sons, Inc., 2011), p. 171.
- <sup>24</sup>H. S. Han, W. Jo, J. Rödel, I. K. Hong, W. P. Tai, and J. S. Lee, *J. Phys.: Condens. Matter* **24**, 365901 (2012).
- <sup>25</sup>R. Dittmer, W. Jo, J. Rödel, S. Kalinin, and N. Balke, *Adv. Funct. Mater.* **22**, 4208 (2012).
- <sup>26</sup>S. V. Kalinin, B. J. Rodriguez, S. Jesse, P. Maksymovych, K. Seal, M. Nikiforov, A. P. Baddorf, A. L. Kholkin, and R. Proksch, *Mater. Today* **11**, 16 (2008).
- <sup>27</sup>A. Kholkin, A. Morozovska, D. Kiselev, I. Bdkin, B. Rodriguez, P. Wu, A. Bokov, Z.-G. Ye, B. Dkhil, L.-Q. Chen, M. Kosec, and S. V. Kalinin, *Adv. Funct. Mater.* **21**, 1977 (2011).
- <sup>28</sup>J. Kreisel, A. M. Glazer, G. Jones, P. A. Thomas, L. Abello, and G. Lucazeau, *J. Phys.: Condens. Matter* **12**, 3267 (2000).
- <sup>29</sup>D. Schütz, M. Deluca, W. Krauss, A. Feteira, T. Jackson, and K. Reichmann, *Adv. Funct. Mater.* **22**, 2285 (2012).
- <sup>30</sup>N. Balke, I. Bdkin, S. V. Kalinin, and A. L. Kholkin, *J. Am. Ceram. Soc.* **92**, 1629 (2009).
- <sup>31</sup>G. Burns and F. H. Dacol, *Solid State Commun.* **48**, 853 (1983).
- <sup>32</sup>V. V. Shvartsman and D. C. Lupascu, *J. Am. Ceram. Soc.* **95**, 1 (2012).
- <sup>33</sup>B. Wylie-van Eerd, D. Damjanovic, N. Klein, N. Setter, and J. Trodahl, *Phys. Rev. B* **82**, 104112 (2010).
- <sup>34</sup>L. Luo, W. Ge, J. Li, D. Viehland, C. Farley, R. Bodnar, Q. Zhang, and H. Luo, *J. Appl. Phys.* **109**, 113507 (2011).
- <sup>35</sup>H. Foronda, M. Deluca, E. Aksel, J. S. Forrester, and J. L. Jones, *Mater. Lett.* **115**, 132 (2014).
- <sup>36</sup>E. Aksel, J. S. Forrester, B. Kowalski, M. Deluca, D. Damjanovic, and J. L. Jones, *Phys. Rev. B* **85**, 024121 (2012).
- <sup>37</sup>M. Acosta, J. Zang, W. Jo, and J. Rödel, *J. Eur. Ceram. Soc.* **32**, 4327 (2012).
- <sup>38</sup>M. I. Mendelson, *J. Am. Ceram. Soc.* **52**, 443 (1969).
- <sup>39</sup>S. Jesse, H. N. Lee, and S. V. Kalinin, *Rev. Sci. Instrum.* **77**, 073702 (2006).
- <sup>40</sup>Y. Liu, Y. Zhang, M.-J. Chow, Q. N. Chen, and J. Li, *Phys. Rev. Lett.* **108**, 078103 (2012).
- <sup>41</sup>H. Zhang, S. Jiang, K. Kajiyoshi, and J. Xiao, *J. Am. Ceram. Soc.* **93**, 750 (2010).
- <sup>42</sup>J. Y. Yi, J.-K. Lee, and K.-S. Hong, *J. Am. Ceram. Soc.* **85**, 3004 (2002).
- <sup>43</sup>M. Hinterstein, M. Knapp, M. Hölzel, W. Jo, A. Cervellino, H. Ehrenberg, and H. Fuess, *J. Appl. Crystallogr.* **43**, 1314 (2010).
- <sup>44</sup>D. Hennings and K. H. Hardtl, *Phys. Status Solidi A* **3**, 465 (1970).
- <sup>45</sup>D. Makovec, Z. Samardžija, U. Delalut, and D. Kolar, *J. Am. Ceram. Soc.* **78**, 2193 (1995).
- <sup>46</sup>R. Shannon, *Acta Crystallogr. A* **32**, 751 (1976).
- <sup>47</sup>A. Popovič, L. Bencze, J. Koruza, B. Malič, and M. Kosec, *Int. J. Mass Spectrom.* **309**, 70 (2012).
- <sup>48</sup>J. König, M. Spreitzer, B. Jančar, D. Suvorov, Z. Samardžija, and A. Popovič, *J. Eur. Ceram. Soc.* **29**, 1695 (2009).
- <sup>49</sup>L. E. Cross, *Ferroelectrics* **76**, 241 (1987).
- <sup>50</sup>W. Jo, S. Schaab, E. Sapper, L. A. Schmitt, H. J. Kleebe, A. J. Bell, and J. Rödel, *J. Appl. Phys.* **110**, 074106 (2011).
- <sup>51</sup>M. Acosta, W. Jo, and J. Rödel, *J. Am. Ceram. Soc.* **97**, 1937 (2014).
- <sup>52</sup>A. A. Bokov and Z. G. Ye, *J. Mater. Sci.* **41**, 31 (2006).
- <sup>53</sup>H. Vogel, *Phys. Z.* **22**, 645 (1921).
- <sup>54</sup>G. S. Fulcher, *J. Am. Ceram. Soc.* **8**, 339 (1925).
- <sup>55</sup>D. Viehland, S. J. Jang, L. E. Cross, and M. Wuttig, *J. Appl. Phys.* **68**, 2916 (1990).
- <sup>56</sup>S. V. Kalinin, B. J. Rodriguez, S. Jesse, A. N. Morozovska, A. A. Bokov, and Z. G. Ye, *Appl. Phys. Lett.* **95**, 142902 (2009).
- <sup>57</sup>W. J. Merz, *Phys. Rev.* **78**, 52 (1950).
- <sup>58</sup>J. Kreisel, A. M. Glazer, P. Bouvier, and G. Lucazeau, *Phys. Rev. B* **63**, 174106 (2001).
- <sup>59</sup>G. M. Rotaru, S. N. Gvasaliya, V. Pomjakushin, B. Roessli, T. Strässle, S. G. Lushnikov, T. A. Shaplygina, and P. Günter, *J. Phys.: Condens. Matter* **20**, 104235 (2008).
- <sup>60</sup>G. A. Samara and E. L. Venturini, *Phase Transfer* **79**, 21 (2006).
- <sup>61</sup>G. A. Samara and L. A. Boatner, *Phys. Rev. B* **61**, 3889 (2000).
- <sup>62</sup>G. A. Samara, *Ferroelectrics* **274**, 183 (2002).
- <sup>63</sup>G. A. Samara, *J. Appl. Phys.* **84**, 2538 (1998).
- <sup>64</sup>G. A. Samara, *Phys. Rev. Lett.* **77**, 314 (1996).
- <sup>65</sup>G. A. Samara, *Ferroelectrics* **117**, 347 (1991).
- <sup>66</sup>J. Gao, Z. Xu, C. Zhang, and X. Yao, *Ferroelectrics* **401**, 86 (2010).
- <sup>67</sup>J. Rouquette, V. Bornand, J. Haines, M. Pintard, and P. Papet, *Ferroelectrics* **288**, 147 (2003).
- <sup>68</sup>S. V. Kalinin, B. J. Rodriguez, J. D. Budai, S. Jesse, A. N. Morozovska, A. A. Bokov, and Z. G. Ye, *Phys. Rev. B* **81**, 064107 (2010).
- <sup>69</sup>Y. Hiruma, Y. Imai, Y. Watanabe, H. Nagata, and T. Takenaka, *Appl. Phys. Lett.* **92**, 262904 (2008).
- <sup>70</sup>J. Petzelt, S. Kamba, J. Fabry, D. Noujni, V. Porokhonsky, A. Pashkin, I. Franke, K. Roleder, J. Suchanicz, and R. Klein, *J. Phys.: Condens. Matter* **16**, 2719 (2004).
- <sup>71</sup>R. Kirchhofer, D. R. Diercks, B. P. Gorman, J. F. Ihlefeld, P. G. Kotula, C. T. Shelton, G. L. Brennecke, and D. J. Green, *J. Am. Ceram. Soc.* **97**, 2677 (2014).
- <sup>72</sup>E. Husson, *Key Eng. Mater.* **155–156**, 1 (1998).